Supporting Information

Atomic Zinc Active Sites on Imine-pyridine Based Covalent Organic Frameworks for Enhancing Photocatalytic H_2O_2 Production

Ruolan Huang,[a] Xuan-He Liu,*[ab] Bing Sun*[a]
[a]*School of Science, China University of Geosciences (Beijing), Beijing 100083, P. R. China.*
[b]*Hubei Key Laboratory of Processing and Application of Catalytic Materials, Huanggang Normal University, Hubei,438000, P. R. China.*
*Corresponding author: liuxh@cugb.edu.cn; sunbing@cugb.edu.cn

Chemicals

Zinc (II) trifluoromethanesulfonate (Zn $(OTf)_2$), nickel (II) trifluoromethanesulfonate (Ni $(OTf)_2$), copper (II) trifluoromethanesulfonate (Cu $(OTf)_2$) were supplied by J&K Chemical.1,3,5-tris(4-aminophenyl) benzene (TAPB) and 6,6'-diformyl-3,3'-bipyridine (BPA) was bought from TCI Chemicals. 1,4-dioxane, mesitylene and acetic acid were purchased by Innochem. All the chemicals are commercially available and used directly without further purification.

Instrumentation

The SEM images were collected on a JSM-7900F thermal field emission scanning electron microscope. The X-ray powder diffraction pattern (XRD) of the photocatalysts were collected by using the PANalytical Empyrean. To obtain the morphology of materials, the transmission electron microscope (TEM) and HRTEM images were measured on a JEM-2100F electron microscope. High-angle annular dark-field scanning TEM (HAADF-STEM) characterization was acquired on a JEM ARM200F thermal field emission microscope. The mass fractions of Zn were determined by ICP-OES (Agilent ICP-OES 5110). UV-vis absorption spectroscopy was performed on UV2600 UV-vis spectrophotometer with $BaSO_4$ as the standard. Fourier transform infrared (FT-IR) spectroscopy was taken on the IR Affinity-1 FTIR spectrometer (Shimadzu, Japan). X-ray photoelectron spectroscopy (XPS) was employed using a ESCALab250Xi instrument. Electron paramagnetic response (EPR) spectra were recorded on a Bruker E500 at room temperature. The apparent quantum yields (AQY) were measured by a calibrated PL-MW2000 optical power meter (PerfectLight, China).

Photoelectrochemical measurements

Photoelectrochemical measurements were conducted using a CHI660E electrochemical workstation equipped with a standard three-electrode system in 0.5 M Na_2SO_4 aqueous solution. A 300 W Xe lamp served as the simulated light source. Ag/AgCl and Pt electrodes were employed as the reference and counter electrodes, respectively. To prepare the working electrode, 5 mg of catalyst was dispersed in a mixture of 1 mL of anhydrous ethanol and 10 μL of Nafion solution via ultrasonic treatment for 30 minutes to form a homogeneous slurry. The resulting slurry was then drop-cast onto FTO glass (1 × 1 cm^2) and dried. The photocurrent was measured under intermittent light illumination at 0.4 V (vs. Ag/AgCl) to record the transient photocurrent response. Electrochemical impedance spectroscopy (EIS) was performed over a frequency range of 0.01 Hz to 10^5 Hz at the same bias potential. Mott-Schottky measurements were carried out at a frequency of 1000 Hz with an amplitude of 10 mV.

Photocatalytic H_2O_2 production

2 mg of photocatalyst was dispersed in 50 mL of deionized water. The suspension was homogenized by ultrasonication while oxygen was continuously bubbled through it to achieve O_2 saturation in the reaction environment. A 300 W Xe lamp (Perfect Light PLS-SEX 300) equipped with an AM 1.5G filter provided simulated solar illumination with an irradiance of 240 ± 5 $mW{\cdot}cm^{-2}$. The concentration of H_2O_2 was quantified using UV-Vis spectrophotometry. Specifically, 1 mL of the reaction mixture was sampled at given time intervals, filtered through a 0.22 μm membrane to remove photocatalyst particles, and then mixed with 2 mM $Ce(SO_4)_2$ solution and 1 mL of deionized water. The H_2O_2 concentration was determined based on the UV spectrophotometric cerium sulfate colorimetric method, as described by equation (1), wherein yellow Ce^{4+} is reduced by H_2O_2 to colorless Ce^{3+}.

$$2Ce^{4+} + H_2O_2 \rightarrow 2Ce^{3+} + 2H^+ + O_2 \qquad (1)$$

The concentration of H_2O_2 was calculated according to equation (2).

$$c(H_2O_2) = ½ \times c(Ce^{4+}) \qquad (2)$$

To establish the calibration curve, a series of standard H_2O_2 solutions with known concentrations were introduced into $Ce(SO_4)_2$ solution, and the corresponding changes in absorption intensity were recorded using a UV/Vis spectrometer. The H_2O_2 concentration in the photocatalytic samples was quantified based on the linear relationship between the concentration of Ce^{4+} and the measured absorbance.

The apparent quantum yield (AQY) of the photocatalysts was measured under irradiation from a 300 W Xenon lamp. The irradiated area of the photocatalytic reactor was approximately 15.9 cm^2. The intensity of the monochromatic light was averaged from measurements taken at five representative locations using a PL-MW2000 photoradiometer. The AQY was then calculated according to equation (3) as follows:

$$\eta\ AQY = \frac{2 \times h \times n \times NA \times c}{S \times P \times t \times \lambda} \times 100\% \qquad (3)$$

n, the Number of H_2O_2 molecules (mol); *h*, Planck constant (6.626×10^{-34} JS); N_A, Avogadro constant (6.022×10^{23} mol^{-1}); *c*, the speed of light (3×10^8 m/s); *S*, the active area of the photocatalytic reactor (cm^2); *P*, irradiation intensity ($W{\cdot}cm^{-2}$); *t*, photoreaction time (s); *λ*, filter wavelength (m).

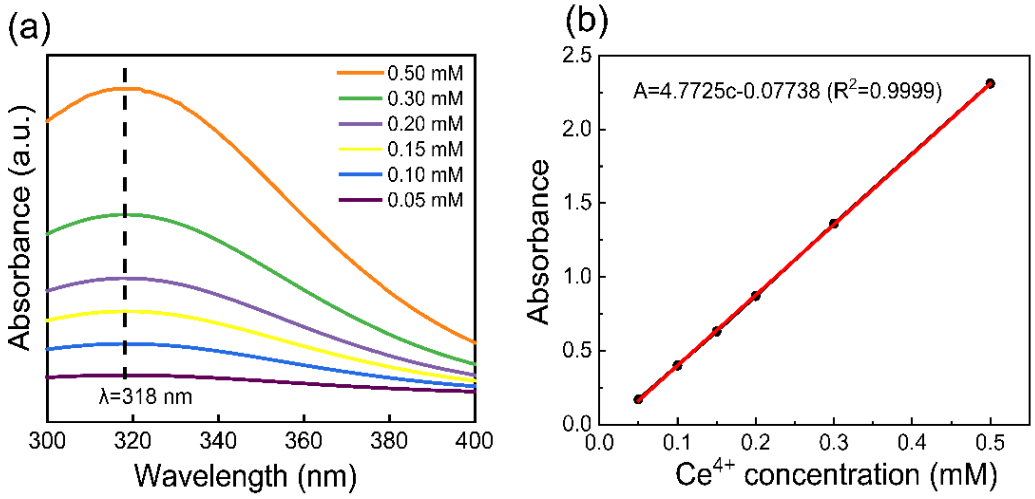

Photocatalytic H_2O_2 decomposition

The aqueous phase was replaced with a 1 mM H_2O_2 solution, while all other experimental steps remained consistent with the procedure described above. The concentration of H_2O_2 for the photocatalyst was then calculated using the following standard Curve:

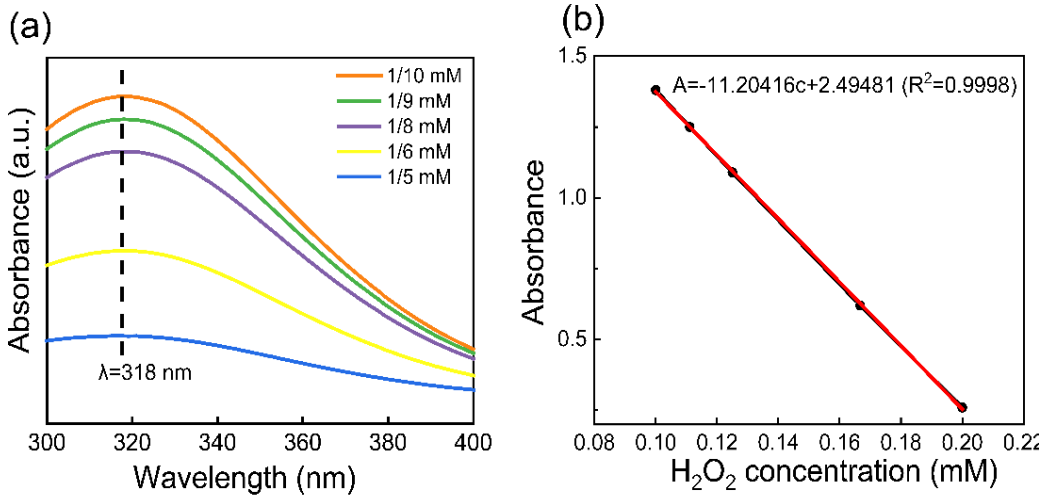

Photocatalytic $\cdot O_2^-$ production

A 2 mg sample of the catalyst was weighed and dispersed into 50 mL of 0.02 mM NBT solution. The solution was purged with O_2 for 30 minutes to saturate it and then irradiated using a 300 W Xe lamp (Perfect Light PLS-SEX 300) equipped with an AM 1.5G filter, which provided simulated solar illumination with an intensity of 240 ± 5 $mW \cdot cm^{-2}$. During irradiation, 2.5 mL aliquots of the reaction solution were periodically taken, and the absorbance at 259 nm was measured to quantify the generation of$\cdot O_2^-$. The O_2^- reduced NBT to a purple formazan precipitate, the absorbance intensity of which is proportional to the$\cdot O_2^-$ concentration. The concentration of H_2O_2 produced was calculated using equation (4):

$$NBT+2\cdot O_2^-+2H^+ \rightarrow Formazan\ (purple)+N_2+2O_2 \quad (4)$$

The concentration of $\cdot O_2^-$ can be calculated by equation (5):

$$c(H_2O_2) = 2 \times c(NBT) \quad (5)$$

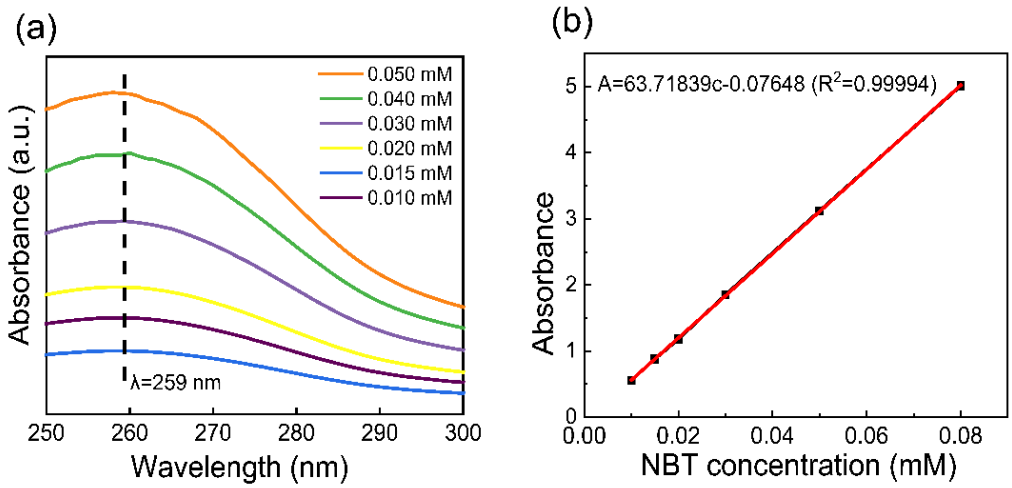

Theoretical calculations

The Vienna Ab Initio Package (VASP) was employed to perform all the density functional theory (DFT) calculations within the generalized gradient approximation (GGA) using the Perdew, Burke, and Enzerhof (PBE) formulation.[1-3] The projected augmented wave (PAW) potentials were applied to describe the ionic cores and take valence electrons into account using a plane wave basis set with a kinetic energy cutoff of 400 eV.[4,5] The DFT calculations employed the PAW pseudopotential library from the VASP package, specifically the PAW_PBE standard library, version 64. Structural modeling and visualization were performed using VESTA software, version 3.5.7. Partial occupancies of the Kohn–Sham orbitals were allowed using the Gaussian smearing method with a width of 0.05 eV. The electronic energy was considered self-consistent when the energy change was smaller than 10^{-5} eV. A geometry optimization was considered convergent when the force change was smaller than 0.05 eV/Å. Grimme's DFT-D3 methodology was used to describe the dispersion interactions.[6] The vacuum spacing perpendicular to the plane of the structure is 20 Å. The dissociation energy is also calculated. The Brillouin zone integral utilized the surfaces structures of 1×1×1 monkhorst pack K-point sampling. Finally, the adsorption energies (E_{ads}) were calculated as $E_{ads}= E_{ad/sub}-E_{ad}-E_{sub}$, where $E_{ad/sub}$, E_{ad}, and E_{sub} are the total energies of the optimized adsorbate/substrate system, the adsorbate in the structure, and the clean substrate, respectively.

The free energy was calculated using the equation (6):

$$G=E_{ads}+ZPE-TS \qquad (6)$$

where G, E_{ads}, ZPE and TS are the free energy, total energy from DFT calculations, zero-point energy and entropic contributions, respectively.

Synthesis procedures

Synthesis of $COF_{TAPB-BPA}$. $COF_{TAPB-BPA}$ was synthesized via acid-catalyzed polycondensation of 1,3,5-tris(4-aminophenyl) benzene (TAPB, 0.08 mmol) and 6,6'-diformyl-3,3'-bipyridine (BPA, 0.12 mmol) in a mixed solvent system of 1,4-dioxane/mesitylene (1 mL, v/v = 1:1). The monomers were placed in a 10 mL Teflon-lined stainless-steel autoclave and sonicated to form a homogeneous celadon suspension. Then, 400 µL acetic acid (6 M) was added as a catalyst. The sealed autoclave was heated at 120 °C for 72 hours. After cooling, the resulting precipitate was collected and washed repeatedly with tetrahydrofuran (THF) to remove any unreacted monomers, followed by further purification via Soxhlet extraction using THF. Finally, the product was activated under dynamic vacuum at 80 °C to afford $COF_{TAPB-BPA}$ as a yellow crystalline powder.

Synthesis of M-$COF_{TAPB-BPA}$. M-COFs were synthesized using a subcomponent assembly strategy based on the aforementioned $COF_{TAPB-BPA}$ protocol. Briefly, $M(OTf)_2$, (M = Zn, Ni, or Cu; 0.08 mmol) were added to the reaction mixture containing TAPB and BPA. All other experimental conditions remained consistent with those used in the parent COF synthesis. The resulting powders were designated as Zn-$COF_{TAPB-BPA}$, Ni-$COF_{TAPB-BPA}$, Cu-$COF_{TAPB-BPA}$, respectively.

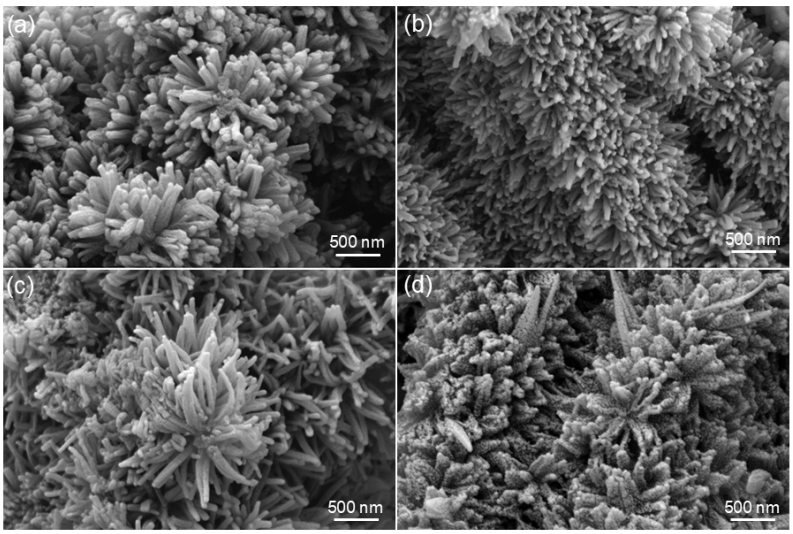

Fig. S1 SEM images of (a)Zn-$COF_{TAPB-BPA}$, (B)Ni-$COF_{TAPB-BPA}$, (C)Cu-$COF_{TAPB-BPA}$, (d)$COF_{TAPB-BPA}$.

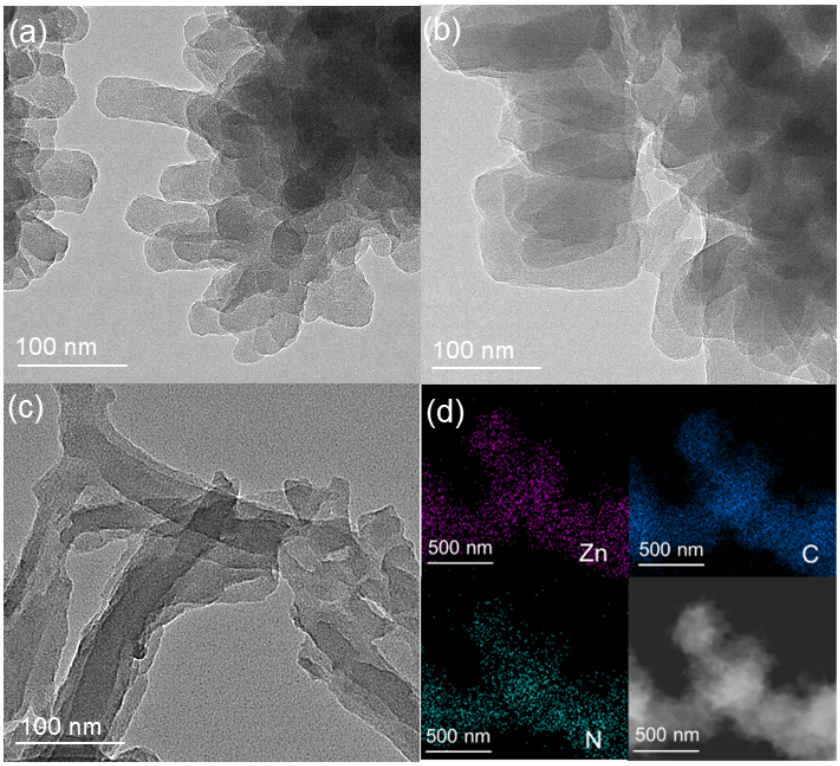

Fig. S2 TEM images of (a)Ni-$COF_{TAPB-BPA}$, (b)Cu-$COF_{TAPB-BPA}$, (c)$COF_{TAPB-BPA}$. (d)EDS images of Zn-$COF_{TAPB-BPA}$

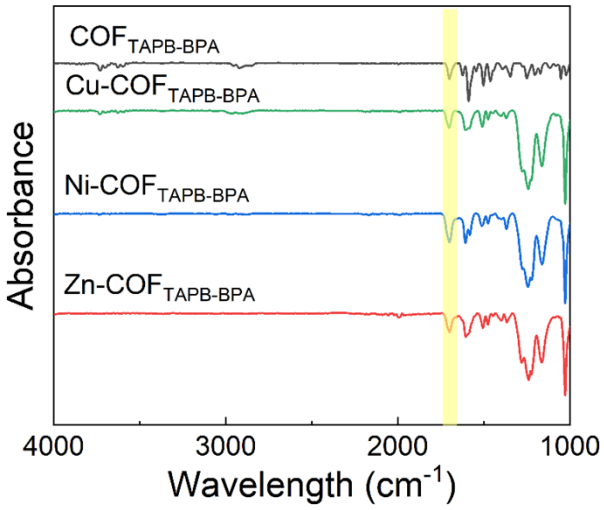

Fig. S3 FT-IR spectra of Zn-COF$_{TAPB-BPA}$, Ni-COF$_{TAPB-BPA}$, Cu-COF$_{TAPB-BPA}$ and COF$_{TAPB-BPA}$.

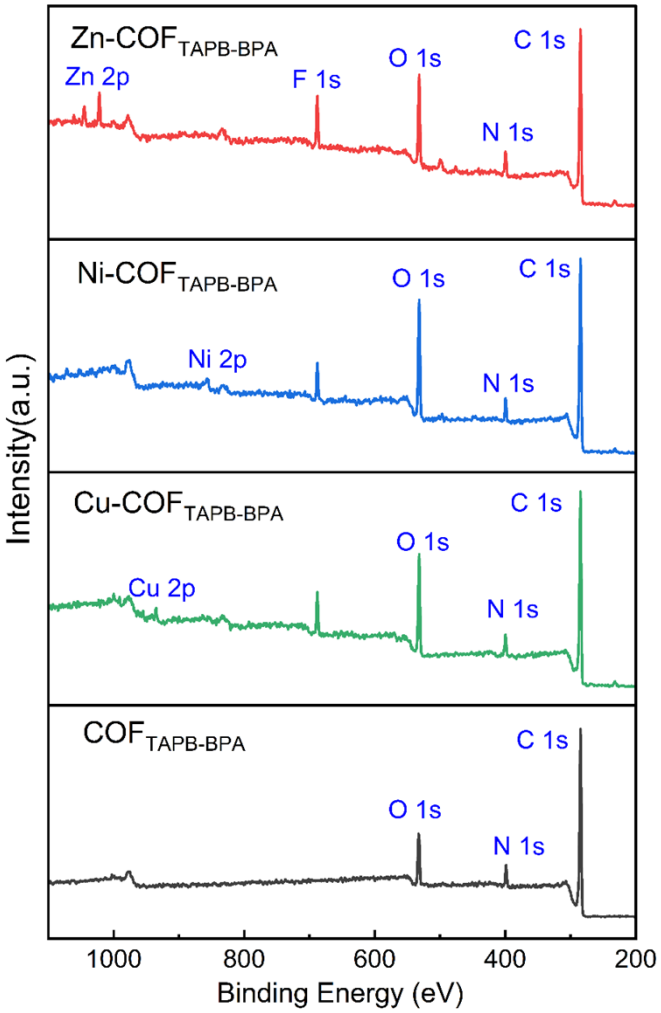

Fig. S4 XPS full spectra of Zn-COF$_{TAPB-BPA}$, Ni-COF$_{TAPB-BPA}$, Cu-COF$_{TAPB-BPA}$ and COF$_{TAPB-BPA}$.

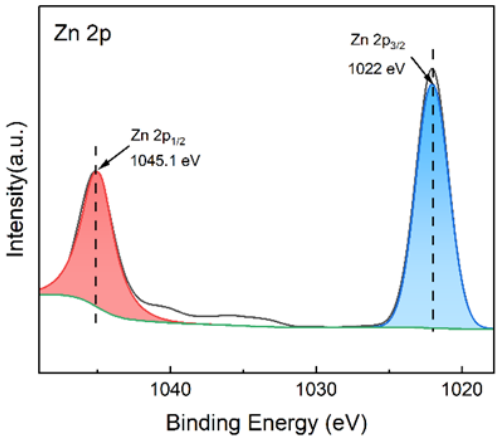

Fig. S5 XPS spectra of Zn 2p for Zn-$COF_{TAPB-BPA}$.

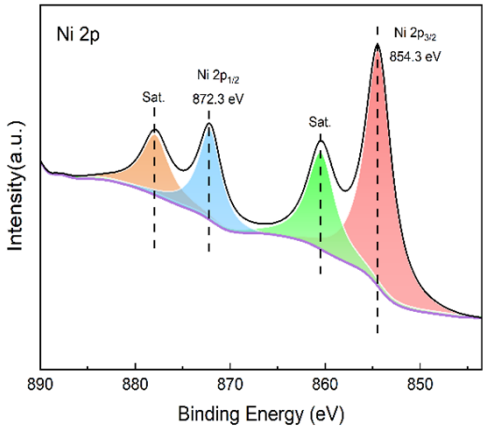

Fig. S6 XPS spectra of Ni 2p for Ni-$COF_{TAPB-BPA}$.

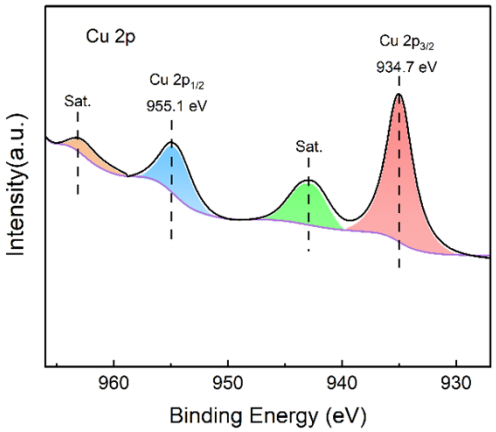

Fig. S7 XPS spectra of Cu 2p for Cu-$COF_{TAPB-BPA}$.

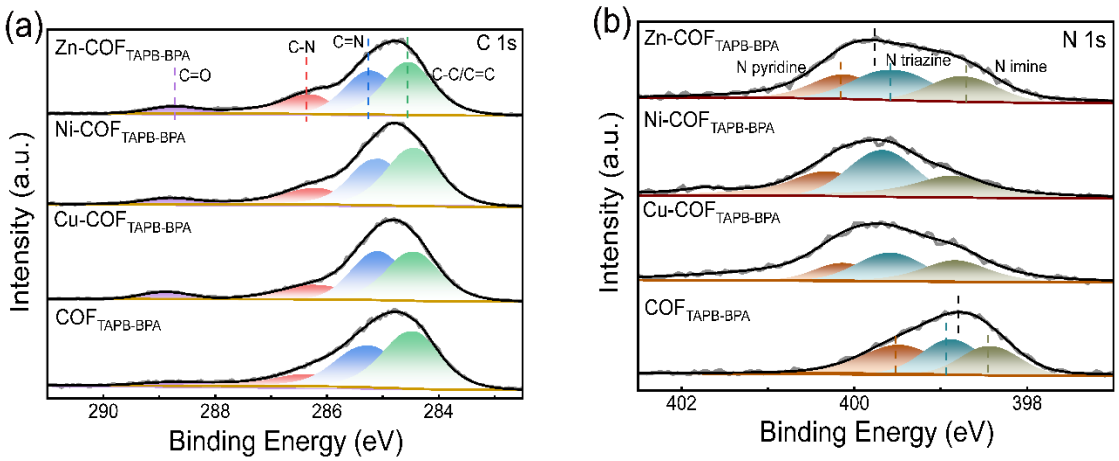

Fig. S8 High resolution XPS spectra of (a) C 1s and (b) N 1s.

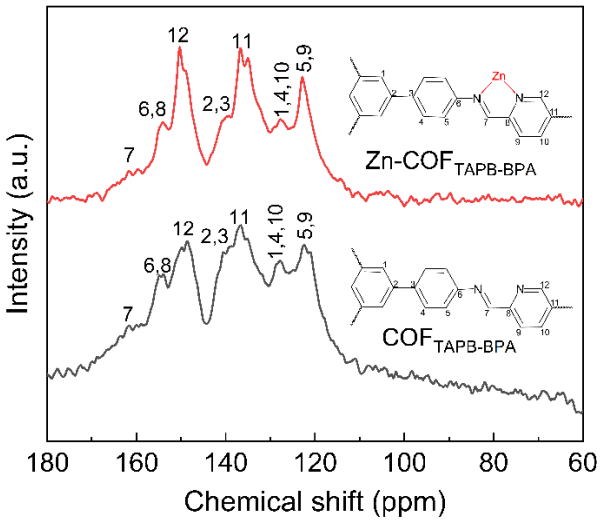

Fig. S9 ^{13}C solid-state NMR spectra of Zn-COF$_{TAPB-BPA}$ and COF$_{TAPB-BPA}$.

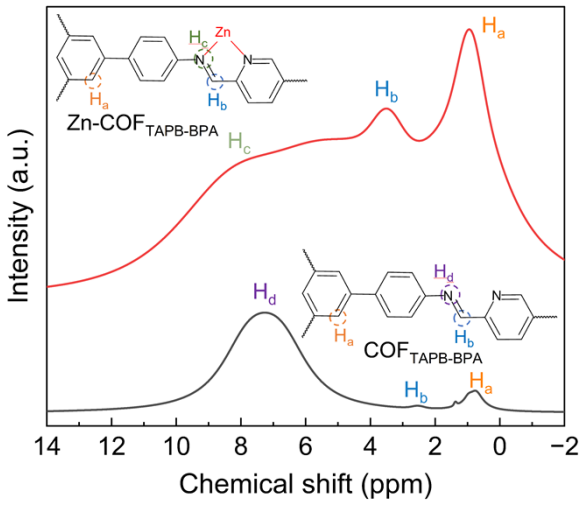

Fig. S10 ^{1}H solid-state NMR spectra of Zn-COF$_{TAPB-BPA}$ and COF$_{TAPB-BPA}$.

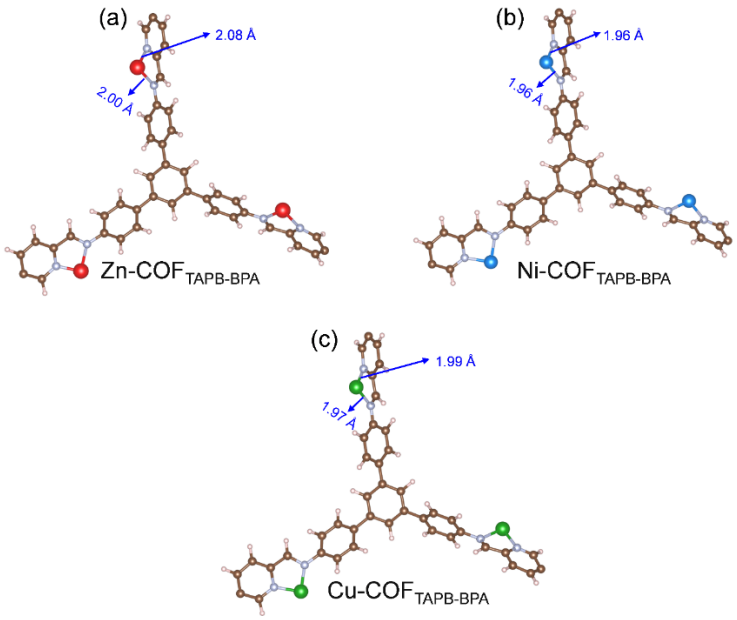

Fig.S11 Metal-nitrogen bonding lengths for optimized structural models of Zn-COF$_{TAPB-BPA}$, Ni-COF$_{TAPB-BPA}$ and Cu-COF$_{TAPB-BPA}$.

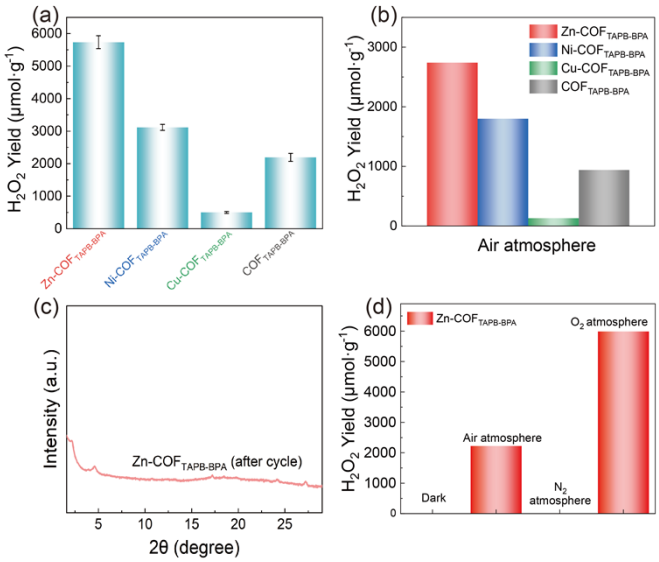

Fig.S12 (a) Photocatalytic H_2O_2 generation with error bars on Zn-COF$_{TAPB-BPA}$, Ni-COF$_{TAPB-BPA}$, Cu-COF$_{TAPB-BPA}$ and COF$_{TAPB-BP}$ under O_2 atmosphere. (b) Air atmosphere using Zn-COF$_{TAPB-BPA}$, Ni-COF$_{TAPB-BPA}$, Cu-COF$_{TAPB-BPA}$ and COF$_{TAPB-BPA}$. (c) XRD pattern of the post-cycling Zn-COF$_{TAPB-BPA}$. (d) Photocatalytic H_2O_2 generation on Zn-COF$_{TAPB-BPA}$ under different conditions.

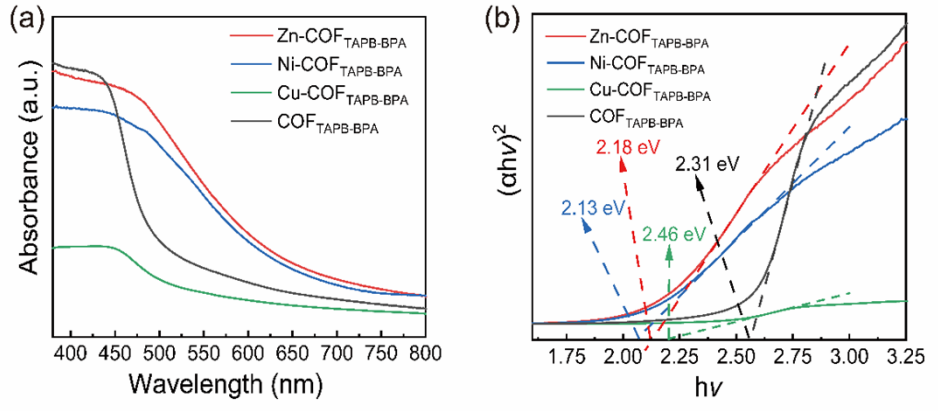

Fig. S13(a) UV-vis absorption spectra, (b) corresponding Tauc-plot band gap of Zn-COF$_{TAPB-BPA}$, Ni-COF$_{TAPB-BPA}$, Cu-COF$_{TAPB-BPA}$ and COF$_{TAPB-BPA}$.

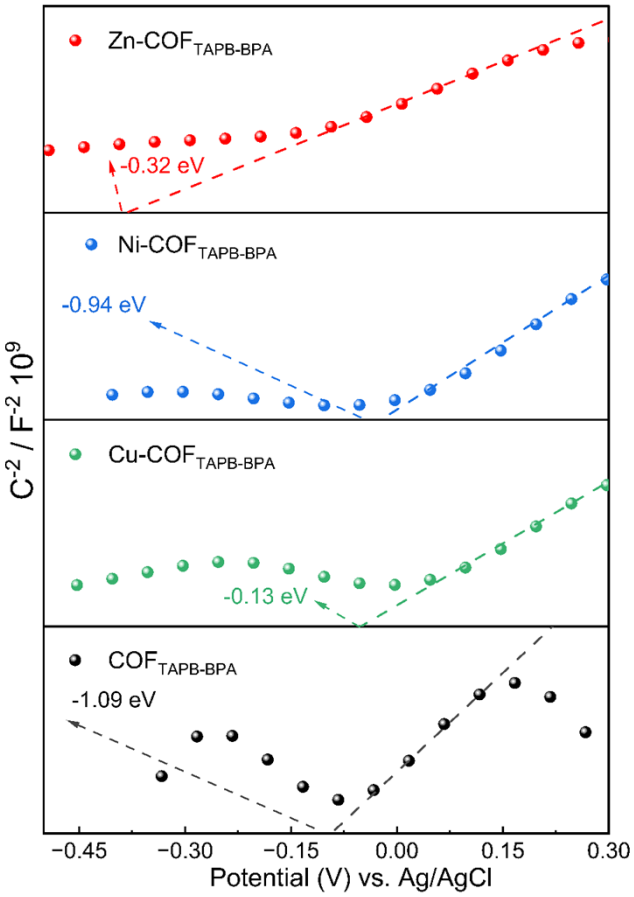

Fig. S14 Mott-Schottky plots of Zn-COF$_{TAPB-BPA}$, Ni-COF$_{TAPB-BPA}$, Cu-COF$_{TAPB-BPA}$ and COF$_{TAPB-BPA}$.

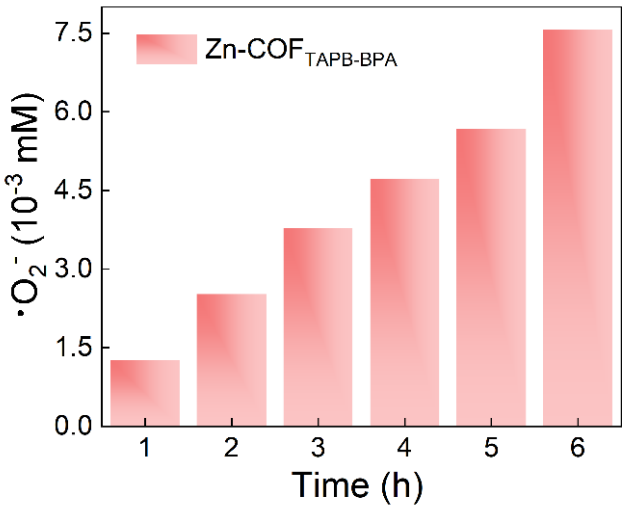

Fig.S15 $\cdot O_2^-$ concentration in the Zn-COF$_{TAPB-BPA}$ photocatalytic system.

Reference

[1] Kresse, G.; Furthmüller, *J. Phys. Rev. B* 1996, 54, 11169-11186.

[2] Perdew, J. P.; Burke, K.; Phys. Rev. Lett. 1996, 77, 3865-3868.

[3] Kresse, G.; Joubert, D. *Phys. Rev. B* 1999, 59, 1758-1775.

[4] Blöchl, P. E. *Phys. Rev. B* 1994, 50, 17953-17979.

[5] Grimme, S.; Antony, J.; Ehrlich, S.; Krieg, H. *J. Chem. Phys.* 2010, 132, 154104.

[6] Henkelman, G.; Uberuaga, B. P.; Jonsson, H. *J. Chem. Phys.* 2000, 113, 9901.